The Astrophysical Journal, 662:199–204, 2007 June 10

THE ENERGY SPECTRUM OF THE BLAZAR MARKARIAN 421 ABOVE 130 GeV

J. E. Carson,[1,2] J. Kildea,[3,4] R. A. Ong,[1] J. Ball,[1] D. A. Bramel,[5,6] C. E. Covault,[7] D. Driscoll,[7] P. Fortin,[8] D. M. Gingrich,[9,10] D. S. Hanna,[3] T. Lindner,[3,11] C. Mueller,[3] A. Jarvis,[1] R. Mukherjee,[8] K. Ragan,[3] R. A. Scalzo,[12,13] D. A. Williams,[14] and J. Zweerink[1]

Received 2006 December 15; accepted 2007 February 28

ABSTRACT

Markarian 421 (Mrk 421) was the first blazar detected at gamma-ray energies above 300 GeV, and it remains one of only twelve TeV blazars detected to date. TeV gamma-ray measurements of its flaring activity and spectral variability have placed constraints on models of the high-energy emission from blazars. However, observations between 50 and 300 GeV are rare, and the high-energy peak of the spectral energy distribution (SED), predicted to be in this range, has never been directly detected. We present a detection of Mrk 421 above 100 GeV as made by the Solar Tower Atmospheric Cherenkov Effect Experiment (STACEE) during a multiwavelength campaign in early 2004. STACEE is a ground-based atmospheric Cherenkov telescope using the wave-front sampling technique to detect gamma rays at lower energies than achieved by most imaging Cherenkov telescopes. We also outline a method for reconstructing gamma-ray energies using a solar heliostat telescope. This technique was applied to the 2004 data, and we present the differential energy spectrum of Mrk 421 above 130 GeV. Assuming a differential photon flux $dN/dE \propto E^{-\alpha}$, we measure a spectral index $\alpha = 2.1 \pm 0.2_{\rm stat}\ ^{+0.2}_{-0.1\ \rm sys}$. Finally, we discuss the STACEE spectrum in the context of the multiwavelength results from the same epoch.

Subject headings: BL Lacertae objects: individual (Markarian 421) — galaxies: active — gamma rays: observations

1. INTRODUCTION

The X-ray-bright, nearby ($z = 0.03$) blazar Markarian 421 was the first extragalactic object detected at very high energies (VHE; $E > 100$ GeV; Punch et al. 1992) and remains one of a dozen VHE detections of blazars to date. Since its discovery, it has produced several major flares, providing many opportunities for multiwavelength campaigns (e.g., Gaidos 1996; Krennrich et al. 1999; Piron et al. 2001; Aharonian et al. 2002). During these periods of days to weeks, it outshines the Crab Nebula by factors of 2–10.

The gamma-ray spectrum of Mrk 421 above 300 GeV has been measured several times at different flux levels, and the VHE spectral index α is known to vary significantly (differential flux $dN/dE \propto E^{-\alpha}$). Krennrich et al. (2002) and Aharonian et al. (2002) made the important observation that the spectral index and the absolute flux level are correlated, suggesting that the high-energy peak of the spectral energy distribution (SED) shifts to higher energies during periods of heightened activity. Also, above a few TeV, a curved deviation from a constant power-law spectrum has been detected for Mrk 421 (Krennrich et al. 2001; Aharonian et al. 2002, 2005).

The simultaneous radio to VHE SED of Mrk 421 has been successfully described in terms of synchrotron self-Compton (SSC) models (Maraschi et al. 1999; Fossati et al. 2000; Krawczynski et al. 2001; Blazejowski et al. 2005). In these models, synchrotron photons from relativistic electrons in the inner regions of the magnetized jet gain energy via inverse-Compton scattering off the same electron population that radiated them. The synchrotron spectrum peaks in the X-ray band, while the inverse-Compton photons are radiated at GeV and TeV energies. Within this framework, the X-ray and TeV data have constrained the magnetic field $\boldsymbol{B}$ and the size R of the gamma-ray emitting region to within factors of a few: $B \sim 0.1$ G and $R \sim 10^{16}$ cm. The measurements are also beginning to constrain the shape of the electron energy distribution and the Doppler factor of the bulk material of the jet, $\delta_{\rm jet} \sim 10$–50.

Although well studied at other energies, the flux of Mrk 421 between 100 and 300 GeV has only been measured three times (Boone et al. 2002; Piron et al. 2003; Albert et al. 2007), and only two measurements have been made of its spectrum around 100 GeV (Piron et al. 2003; Albert et al. 2007). Measurements in this wave band are of particular scientific interest, because most SSC models predict that the high-energy SED will peak around 100 GeV. Testing this prediction can place valuable constraints on the various electron emission models, especially in describing the energy distribution of the relativistic electrons.

We report the detection of Mrk 421 above 100 GeV using the Solar Tower Atmospheric Cherenkov Effect Experiment (STACEE;

[1] Department of Physics and Astronomy, University of California, Los Angeles, Los Angeles, CA 90095.
[2] Current address: Stanford Linear Accelerator Center, Menlo Park, CA 94025.
[3] Department of Physics, McGill University, Montreal, QC H3A 2T8, Canada.
[4] Current address: Fred Lawrence Whipple Observatory, Harvard-Smithsonian Center for Astrophysics, Amado, AZ 85645.
[5] Department of Physics, Columbia University, New York, NY 10027.
[6] Current address: Interactive Brokers, One Pickwick Plaza, Greenwich, CT 06830.
[7] Department of Physics, Case Western Reserve University, Cleveland, OH 44106.
[8] Department of Physics and Astronomy, Barnard College, Columbia University, New York, NY 10027.
[9] Department of Physics, University of Alberta, Edmonton, AB T6G 2G7 Canada.
[10] Also at TRIUMF, Vancouver, BC V6T 2A3 Canada.
[11] Current address: Department of Physics and Astronomy, University of British Columbia, Vancouver, BC V6T 1Z1, Canada.
[12] Department of Physics, University of Chicago, Chicago, IL 60637.
[13] Current address: Lawrence Berkeley National Laboratory, Berkeley, CA 94720.
[14] Santa Cruz Institute for Particle Physics, University of California, Santa Cruz, Santa Cruz, CA 95064.

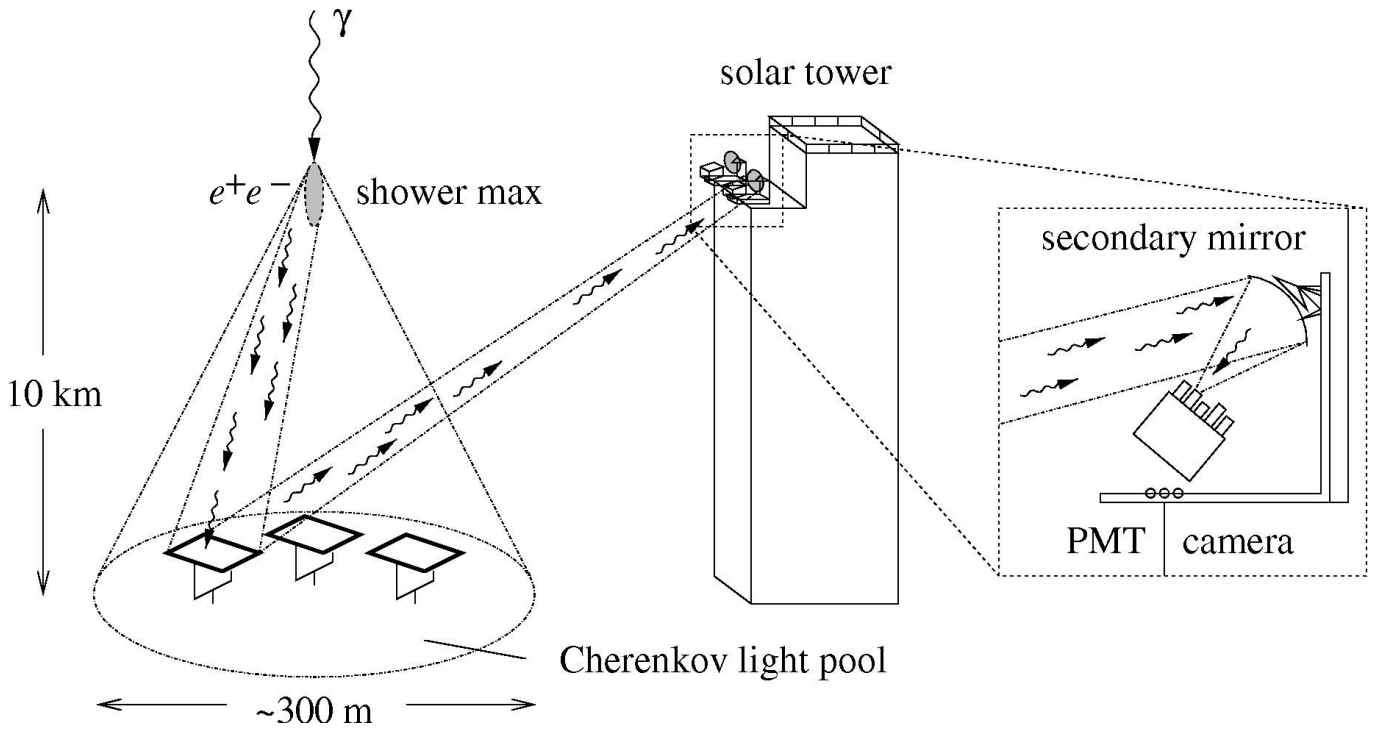

FIG. 1.—Schematic representation of the wave-front sampling technique. A gamma ray incident on the atmosphere induces an air shower that illuminates an area approximately 300 m in diameter on the ground with Cherenkov light. The light is reflected by heliostat mirrors onto secondary mirrors and then focused onto PMTs mounted on cameras under the secondaries.

Gingrich et al. 2005) and present a measurement of the integral flux and differential energy spectrum between 130 GeV and 2 TeV. Section 2 briefly describes the STACEE experiment itself and the Mrk 421 data set. Section 3 presents the basic data analysis, and § 4 presents the integral flux results. Section 5 describes the spectral analysis and results, and § 6 discusses the scientific implications of the results.

2. STACEE OBSERVATIONS

STACEE is a ground-based atmospheric Cherenkov telescope that utilizes the wave-front sampling technique (Smith 2005) to measure gamma rays above about 100 GeV. Gamma rays and cosmic rays striking the Earth's atmosphere induce extensive air showers, and Cherenkov light is one product of the showers. The Cherenkov light pool typically illuminates an area approximately 300 m in diameter on the ground. In the wave-front sampling technique as employed by STACEE, the Cherenkov light is focused by heliostat mirrors, large reflectors built originally for solar energy research, onto secondary mirrors and then onto photomultiplier tubes (PMTs). The digitized PMT signals form the raw data product. There is one PMT viewing each heliostat, so the technique samples the Cherenkov wave front at the location of each heliostat. Figure 1 illustrates this technique. A key feature of all atmospheric Cherenkov detectors is that the effective collecting area for high-energy gamma rays is much larger than the physical size of the mirrors used to collect the Cherenkov light. Wave-front sampling detectors like STACEE, which use large heliostats as opposed to focusing dishes, have larger mirror areas and can therefore work at lower gamma-ray energies where Cherenkov photon densities on the ground are lower.

STACEE uses 64 of the 220 heliostats at the National Solar Thermal Test Facility in Albuquerque, New Mexico. These 64 reflectors are distributed fairly evenly over an area of $\sim 150 \times 240$ m. Each heliostat is composed of a 5×5 array of square mirror facets, and each facet has a collecting area of 1.5 m^2. The light from a heliostat is reflected onto one of five secondary mirrors. Three large secondaries ($\sim$2 m in diameter) focus light onto one of three cameras holding 16 PMTs each, and two smaller secondaries ($\sim$1.1 m in diameter) focus light onto one of two smaller cameras holding eight PMTs each. STACEE also operates a custom-made atmospheric monitoring system during observations. This system includes a weather station and a photometer for measuring atmospheric transmission.

The signal from each PMT is fanned out to a discriminator and to an eight-bit flash analog-to-digital converter (FADC). The FADCs continuously digitize the 64 PMT signals with a sampling rate of 1 sample ns^{-1}; a typical Cherenkov pulse is several nanoseconds wide, so these digitizers record the shape of each pulse. The pulse shape information from the FADCs allows precise pulse times and sizes to be extracted. Relative pulse timing is used to reconstruct the direction of the gamma ray, and pulse sizes are used to reconstruct gamma-ray energy. A set of dynamic delays ensures that the 64 pulses remain synchronized as the source is followed across the sky.

The Cherenkov light from air showers arrives on the ground as a "pancake" a few nanoseconds thick, and over that brief interval it is brighter than the night sky background. STACEE employs a two-level trigger system and a tight timing coincidence requirement to pick out Cherenkov-emitting air showers from the night sky glow. The trigger system is designed as follows. First, the heliostats are grouped geographically into eight clusters of eight heliostats each. The cluster-level, or L1, trigger requires that the signals from five of the eight heliostats within a cluster pass the discriminator threshold, typically about four photoelectrons, within a timing window of 8–24 ns. Then, the array-level, or L2, trigger requires that five of the eight clusters generate an L1 trigger within a 16 ns window. When the L2 trigger condition is satisfied, the digitized traces from all 64 PMTs are recorded.

The vast majority of the air showers detected by STACEE are initiated by protons or light nuclei. In order to extract a gamma-ray signal from data dominated by this cosmic-ray background, STACEE employs an "on-off" observing strategy in which each 28 minute on-source observation is paired with an equal exposure off-source observation. The off-source observation is at the same declination as the on-source observation and is 30′ (7.5°) away in right ascension, so it covers the same trajectory in local sky coordinates. The number of cosmic-ray events in the off-source observation is subtracted from the number of on-source events to find the statistical excess of gamma-ray events from the direction of the source. Many on-off pairs of observations for a given source taken over several weeks are used together to establish a gamma-ray signal from that source. The observations of Mrk 421 presented here were taken on 18 nights from 2004 January 29 to May 15. The total on-source exposure time was 20.5 hr, with an equal amount of off-source exposure time.

3. ANALYSIS

A set of criteria was applied to the data set to select and remove all periods of time with unreliable data. First, data taken during a hardware malfunction were removed. These malfunctions included mispointings of one or more heliostats, trips of the high-voltage power to the PMTs, or failures of the data acquisition system. Second, the weather station data were checked for evidence of frost, which can accumulate on the heliostats and seriously degrade their reflectivities. A total of 5.7 hr of data was removed due to hardware malfunctions and frost.

Data were also removed if marred by changes in background light levels, e.g., from clouds drifting through the field of view or from lights from cars or airplanes passing near the experiment. The observable quantities used to identify these time periods were the L1 trigger rates. For every observing run, the L1 rates were examined by eye and were required to vary smoothly during a run (i.e., no sudden spikes or drops). The stability of the L1 and L2 rates were verified in the post-cut data. This step eliminated an additional 5.7 hr of on-source data. After all data quality cuts, the final data set comprised 9.1 hr of on-source data taken on 16 nights.

Before the on- and off-source observations could be compared to determine the statistical excess of gamma-ray events, an important correction was made to account for the effects of the different background light levels between the on- and off-source sky fields. These differences are largely due to the particular stars in those fields; a single bright star in one of the fields can radically alter the light level. Low-energy cosmic-ray showers that are just below the threshold required to initiate an event trigger can be promoted above threshold by large positive fluctuations of the night sky background. Likewise, showers that are just above threshold can be demoted by large negative background fluctuations. If there were an equal number of showers at all energies, then there would be the same number of showers promoted above threshold as demoted below threshold. However, because there are more low-energy showers than high-energy ones (the cosmic-ray spectrum decreases with increasing energy), the net effect of the night sky background fluctuations is to promote subthreshold showers. This effect leads to a higher cosmic-ray rate in observations with brighter sky fields. If the area of sky covered by the on-source observation is brighter than that of the off-source observation, as is the case for Mrk 421, then this effect can imitate a true gamma-ray signal.

A technique called "padding" (Scalzo et al. 2004) has been developed to equalize the background light levels in a two-step process. The technique relies on a precompiled library of FADC waveforms corresponding to various low light levels measured under controlled conditions. In the first step, background noise from this library is added to "pad" the FADC waveforms of the observation with the dimmer background. This step equalizes the rms fluctuations, measured from the 400 ns preceding the pulse itself, between the on- and off-source observations. In the second step, the trigger condition is reimposed at a higher discriminator threshold. This is necessary because the showers in the dimmer background observation that *would* have triggered the detector if the light levels had been equal are absent from the data stream. Imposing a software trigger identical to the hardware trigger cannot regain these lost showers. Therefore, the threshold is raised in software to the level where the dimmer background observations are not missing promoted showers relative to the brighter background observations. The technique is fully described in Scalzo et al. (2004), Scalzo (2004), and Carson (2005).

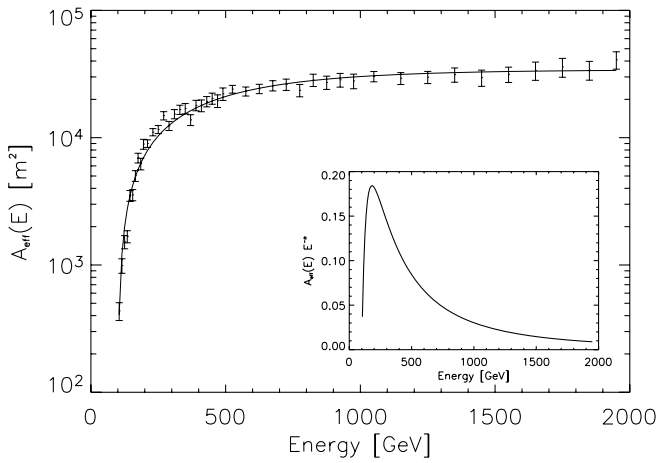

FIG. 2.—Effective area, the overall collecting area of the experiment, for the Mrk 421 data set. The data points represent an exposure-weighted average over simulated observations at five different zenith angles, and the solid line is a fit to the form $A_0\left[1 - e^{-(E-E_{\min})/E_r}\right]$ where A_0, $E_{\min}$, and E_r are constants. $E_{\min}$ is the minimum energy simulated (100 GeV), and E_r is the characteristic energy of the sharp rise in the effective area. *Inset*: The (unnormalized) differential trigger rate as a function of energy for a spectral index $\alpha = 2.0$. The energy threshold is defined as the peak of this curve (180 GeV).

4. INTEGRAL FLUX RESULTS

After applying the quality cuts and field brightness correction, there are 2897 excess events in 511.3 minutes for a photon count rate of 5.7 ± 0.9 photons minute^{-1}. The detection significance is 5.9 standard deviations above the background. The mean significance per observed pair is 1.4 σ in 28 minutes of on-source exposure time.

The detector response is characterized by the effective area $A_{\rm eff}$, defined as the overall gamma-ray collecting area of the experiment, as opposed to the physical area of the heliostat mirrors. It is determined from Monte Carlo simulations of the air shower physics and the detector performance, as described in Scalzo et al. (2004) and Bramel et al. (2005). The effective area for the Mrk 421 data set is shown in Figure 2. The data points reflect simulations of observations at five different zenith angles, exposure weighted to reflect the composition of the real data set. The solid line is a fit to the data assuming $A_{\rm eff} = A_0\left[1 - e^{-(E-E_{\min})/E_r}\right]$, where A_0, $E_{\min}$, and E_r are constants.

The differential trigger rate dR/dE (photons s^{-1} GeV^{-1}) is $A_{\rm eff}$ times the differential photon flux dN/dE, expressed as a power law:

$$\frac{dN}{dE} = N_0 \left(\frac{E}{E_0}\right)^{-\alpha} .$$

Assuming a spectral index $\alpha = 2.0$, the curve of $A_{\rm eff}E^{-\alpha}$ for the Mrk 421 data set, which is proportional to the differential trigger rate, is shown in the inset to Figure 2.

Following the usual convention in VHE astronomy, we define the energy threshold as the energy of the peak of the differential rate curve. From Figure 2, the peak is at $E_{\rm th} = 180$ GeV. It is clear from the figure that, like all VHE instruments, STACEE has significant sensitivity to energies below $E_{\rm th}$, as defined in this way. The systematic error on the STACEE energy scale is estimated to be ~20% (Scalzo 2004). Assuming $\alpha = 2.0$, the integral flux of VHE gamma rays from Mrk 421 measured by STACEE is $\Phi(E > 180\ {\rm GeV}) = (4.7 \pm 0.8_{\rm stat}) \times 10^{-10}$ photons cm^{-2} s^{-1}.

5. SPECTRAL ANALYSIS AND RESULTS

We have developed a technique for reconstructing gamma-ray energies from the charges recorded on each of the 64 PMTs that constitute the STACEE camera. The method relies on two physical properties of gamma-ray showers: (1) the intensity of the Cherenkov light on the ground is directly proportional to the energy of the initiating gamma ray, and (2) the light distribution on the ground is approximately uniform out to the edges of the shower. These properties, along with an independent estimate of the shower core location (Scalzo 2004), allow us to convert a PMT charge to a number of photons arriving at the corresponding heliostat. This conversion relies on simulations of the STACEE electronics and optics that have been thoroughly checked against calibration data (Scalzo 2004; Carson 2005). The reconstructed lateral photon distribution is then converted to a gamma-ray energy using standard simulations of air showers initiated by gamma rays. The energy reconstruction method successfully reconstructs the energies of simulated gamma rays between 130 GeV and ~2 TeV with an energy resolution of 20%–30%; systematic errors in the energy estimate are less than 10%. The details of the technique are described in Carson (2005). It was applied to STACEE data taken on the Crab Nebula, the standard calibration source for VHE astronomy, and the results are in good agreement with previous measurements (Hillas et al. 1998; Aharonian et al. 2004; Wagner et al. 2005).

The energy reconstruction method was also applied to the 2004 Mrk 421 data. The reconstructed energies were sorted into six energy bins: 130–150 GeV, 150–200 GeV, 200–300 GeV, 300–500 GeV, 500–1000 GeV, and >1 TeV. The bin choices were motivated by two considerations: (1) ensuring that the effective area did not change substantially over the bin, and (2) having a similar number of entries in each bin. For each energy bin, the number of deadtime-corrected entries in the off-source observations was subtracted from the number of deadtime-corrected entries in the on-source observations, and the gamma-ray excess in each energy bin was divided by the livetime for the observations and the time-averaged effective area at that energy. The resulting differential spectrum dN/dE (photons cm^{-2} s^{-1} GeV^{-1}) is shown in Figure 3. Fitting the spectrum with the power law from § 4 with $E_0 = 100$ GeV, we find

$$N_0 = (9.6 \pm 3.5_{\rm stat}\ ^{+3.1}_{-2.0\ {\rm sys}}) \times 10^{-12}\ {\rm photons\ cm^{-2}\ s^{-1}\ GeV^{-1}}$$

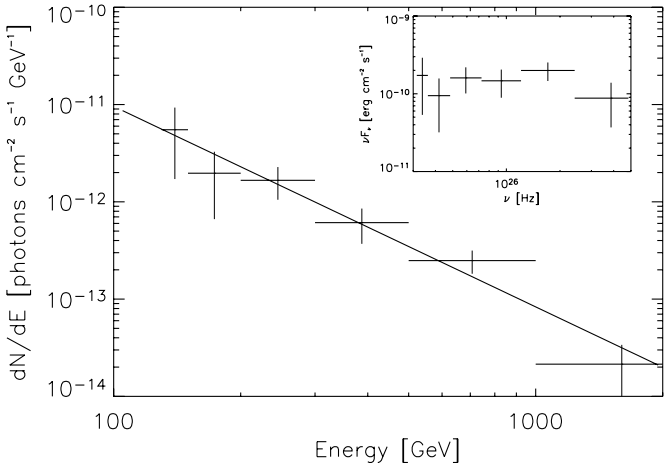

FIG. 3.—Mrk 421 spectrum between 130 GeV and 2 TeV, as measured by STACEE in early 2004. The spectral index is $\alpha = 2.1 \pm 0.2_{\rm stat}\ ^{+0.2}_{-0.1\ {\rm sys}}$. The vertical error bars represent the statistical errors in both the signal and the effective area. The horizontal bars represent the widths of the energy bins. *Inset*: The same spectrum plotted using the standard convention, as $\nu F_\nu = E^2\, dN/dE$ (ergs cm^{-2} s^{-1}) vs. frequency ν.

and

$$\alpha = 2.1 \pm 0.2_{\rm stat}\ ^{+0.2}_{-0.1\ {\rm sys}}.$$

In the inset to Figure 3, the Mrk 421 SED is plotted as $\nu F_\nu = E^2\, dN/dE$ (ergs cm^{-2} s^{-1}).

We note that absorption by the extragalactic background light (EBL) will have only a small effect on the spectrum of such a nearby source ($z = 0.03$) for energies below a few hundred GeV. Therefore, we have not corrected for absorption effects in this analysis. However, EBL absorption can affect the spectrum at higher energies, shifting the observed peak to lower energies than the source's true inverse-Compton peak. We bear this in mind in the discussion that follows.

6. DISCUSSION

As shown in the inset to Figure 3, the Mrk 421 SED is flat in the STACEE band. The STACEE measurement suggests that the observed high-energy peak of the SED of Mrk 421 was at or above 130 GeV ($\log \nu = 25.5$) in early 2004. This is a slightly higher energy for the peak than predicted by most SSC models, such as the time-dependent SSC model of Krawczynski et al. (2001), which predicts a high-energy peak of between 10 and 100 GeV. A shift of the high-energy peak above 100 GeV is sometimes invoked in modeling of bright flares, however; for instance, Maraschi et al. (1999) suggested that the peak shifted to several hundred GeV during a flare in 1998 April.

The STACEE observations of Mrk 421 were part of an extensive multiwavelength campaign; during the first 5 months of 2004 the source was monitored by radio, optical, X-ray (*RXTE*), and TeV (Whipple) telescopes simultaneously. These multiwavelength measurements were presented in Figure 12 of Blazejowski et al. (2005) and are summarized here. The data were divided into "medium" and "high" states of activity based on their X-ray fluxes. It turned out that this division separated the data into two time periods; the medium state covers the period from 2004 January 27 to March 26, and the high state covers 2004 April 16–20. The medium- and high-state data were fit to one- and two-zone SSC models, respectively, where a zone is a spherical emitting

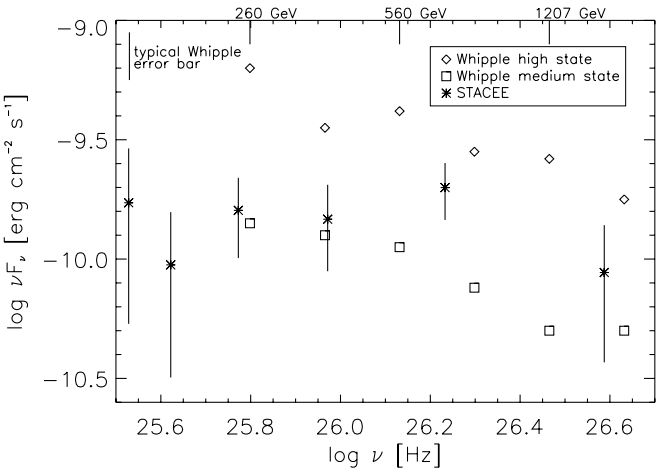

FIG. 4.—Spectral energy distributions of Mrk 421 from Whipple (*open squares and diamonds*) and STACEE (*stars*). The former are divided into medium (*open squares*) and high (*open diamonds*) states of activity based on their X-ray flux, as in Blazejowski et al. (2005). A typical Whipple error bar is shown in the upper left corner.

region characterized by a single magnetic field and electron population. These models (Krawczynski et al. 2004) are snapshots of the SSC radiation emitted by a steady-state electron population, and do not evolve the electron spectrum self-consistently. Power-law fits were performed on the Whipple data assuming a high-energy cutoff of 4.96 TeV; these fits returned spectral indices of 2.40 ± 0.18 and 2.11 ± 0.14 for the medium- and high-state data, respectively. The STACEE data set covers about 40% of the nights represented in the multiwavelength SED (Fig. 12 of Blazejowski et al. 2005), and ~90% of the STACEE data set was taken during these nights. Approximately 25% of the STACEE data were from the TeV flaring state in April.

The STACEE spectral index is consistent with the high-state spectral index determined by Whipple and marginally consistent with the medium-state spectral index. However, it is naive to expect the spectrum to follow a simple power law over such a large range in energy, and the most useful comparison of the two data sets is restricted to the energy range where they overlap, as shown in Figure 4. The open symbols are the Whipple data from the high (*diamonds*) and medium (*squares*) states. The STACEE spectrum is shown as asterisks. We note that the first STACEE energy bin is at 140 GeV, 120 GeV lower than the first Whipple energy bin. Figure 4 shows that the STACEE and Whipple measurements are in good agreement, especially considering that no cross-calibration was performed on the data from the two instruments and that the errors shown are statistical only. We expect the STACEE flux levels to coincide more closely with the Whipple measurements in the medium state, as seen, since the majority of the STACEE data were taken before the 2004 April flare. The STACEE data show that the spectrum remains approximately flat down to an energy of 130 GeV.

The most consistent interpretation of the combined STACEE and Whipple data is that the observed peak of the SED is around 130–500 GeV ($\log \nu \sim 25.5$–26.1). Of course, the true inverse-Compton peak may be even higher, if EBL absorption is contributing to the falloff above 500 GeV. This is a higher peak energy than expected from past modeling for a medium flux state, including the SSC model shown in Blazejowski et al. (2005). We note, however, that the Blazejowski et al. (2005) medium-state model overpredicts the Whipple data at the lowest energies, and a peak in the range indicated above is a better reflection of the data than the one-zone model peak. A detection of the peak indicates that we are measuring most of the energy released in inverse-Compton cooling, and constrains the inverse-Compton peak energy much more than a measurement of the falling edge of the SED alone. Going a step further and combining the VHE data with the X-ray data near the synchrotron peak then measures the total energy budget of Markarian 421 and the relative contributions of synchrotron and inverse-Compton cooling. During the period of these observations, the combined STACEE and X-ray data suggest that the synchrotron peak was a factor of 2–3 higher than the inverse-Compton peak, suggesting that synchrotron cooling dominates. Because these data represent a time average of the jet radiation, we suggest further modeling that evolves the electron population as it cools via synchrotron radiation.

During the preparation of this manuscript we learned of a measurement of the Mrk 421 energy spectrum by the MAGIC collaboration (Albert et al. 2007). The energy range covered by MAGIC includes much of that explored by STACEE, and they also report a flattening of the energy spectrum at the low end. Their data are from a different epoch (2004 November to 2005 April), so a direct comparison of data sets from this highly episodic source is not easily made. However, it is clear that many such observations will help with the detailed understanding of Mrk 421.

In summary, we have measured a spectrum of Markarian 421 above 130 GeV in six energy bins. The STACEE data suggest that we are detecting the high-energy peak of the observed SED for the first time above 100 GeV, and that the inverse-Compton peak is around 130–500 GeV, or possibly higher, depending on the EBL density. The direct detection of the observed peak can strongly constrain future modeling.

We are grateful to the staff at the National Solar Thermal Test Facility, who continue to support our science with enthusiasm and professionalism. This work was supported in part by the National Science Foundation, the Natural Sciences, and Engineering Research Council of Canada (NSERC), Fonds Québécois de la Recherche sur la Nature et les Technologies (FQRNT), the Research Corporation, and the University of California at Los Angeles.

REFERENCES

Aharonian, F., et al.. 2002, A&A, 393, 89
———. 2004, ApJ, 614, 897
———. 2005, A&A, 437, 95
Albert, J., et al. 2007, ApJ, in press (astro-ph/0603478)
Blazejowski, M., et al. 2005, ApJ, 630, 130
Boone, L. M., et al. 2002, ApJ, 579, L5
Bramel, D. A. et al. 2005, ApJ, 629, 108
Carson, J. E. 2005, Ph.D. thesis, Univ. California, Los Angeles
Fossati, G., et al. 2000, ApJ, 541, 166
Gaidos, J. A. 1996, Nature, 383, 319
Gingrich, D. M., et al. 2005, IEEE Trans. Nucl. Sci, NS-52, 2977
Hillas, A. M., et al. 1998, ApJ, 503, 744
Krawczynski, H., et al. 2001, ApJ, 559, 187
———. 2004, ApJ, 601, 151
Krennrich, F., et al. 1999, ApJ, 511, 149
———. 2001, ApJ, 560, L45
———. 2002, ApJ, 575, L9
Maraschi, L., et al. 1999, ApJ, 526, L81

Piron, F., et al. 2001, A&A, 374, 895
———. 2003, in Proc. 28th Int. Cosmic Ray Conf. (Tsukuba), 5, 2607
Punch, M., et al. 1992, Nature, 358, 477
Scalzo, R. A. 2004, Ph.D. thesis, Univ. Chicago
Scalzo, R. A., et al. 2004, ApJ, 607, 778
Smith, D. A. 2005, in Towards a Network of Atmospheric Cherenkov Detectors VII, ed. B. Degrange & G. Fontaine (Palaiseau: Ecole Polytechnique), 67
Wagner, R. M., et al. 2005, in Proc. 29th Int. Cosmic Ray Conf. (Mumbai), 4, 163